

Article

Pattern Classification and Gear Design of Spatial Noncircular Gear Continuously Variable Transmission

Yongquan Yu ¹, Chao Lin ^{1,*}  and Ping Xu ²

¹ State Key Laboratory of Mechanical Transmission, Chongqing University, Chongqing 400044, China; 20160702017@cqu.edu.cn

² Chongqing Panlian Transmission Technology Co., Ltd., Chongqing 400060, China; xuping_cq@126.com

* Correspondence: linchao@cqu.edu.cn; Tel.: +86-134-529-11958

Abstract: Noncircular gear and curve face gear are collectively referred to as spatial noncircular gear. Combined with the transmission characteristics of spatial noncircular gear, a new classification design method of spatial noncircular gear continuously variable transmission (CVT) pattern was proposed, including two categories named addition type and multiplication type, with a total of five subcategories. Through the combination of the transmission ratio changing mechanism and transmission selection mechanism, it can realize the CVT. The overall transmission ratio depends on the phase angle between the spatial noncircular gear pairs and is independent of the input rotation angle. Firstly, the CVT principle and transmission ratio characteristics of each pattern were analyzed. Then the tooth profile classification design of spatial noncircular gear was carried out, and the general parametric design equations of the tooth surface with different tooth profiles were obtained. Finally, through simulation, the overall transmission ratio of each pattern was compared between theory and simulation, which verified the correctness of the CVT classification design method. The advantages and disadvantages of the two categories were analyzed. Moreover, through the transmission experiments of curve face gear pairs with different tooth profiles, the transmission ratios were compared between theory and experiment. Considering the influencing factors such as machining error, assembly error and measurement error, the experimental error is within a reasonable error range, which verified the correctness of the tooth profile classification design method. This study provides a new idea for the further research and application of spatial noncircular gear CVT.

Keywords: CVT pattern; general equation; simulation and experiment; spatial noncircular gear; tooth profile classification design



Citation: Yu, Y.; Lin, C.; Xu, P. Pattern Classification and Gear Design of Spatial Noncircular Gear Continuously Variable Transmission. *Appl. Sci.* **2022**, *12*, 2715. <https://doi.org/10.3390/app12052715>

Academic Editor: César M. A. Vasques

Received: 12 February 2022

Accepted: 3 March 2022

Published: 5 March 2022

Publisher's Note: MDPI stays neutral with regard to jurisdictional claims in published maps and institutional affiliations.



Copyright: © 2022 by the authors. Licensee MDPI, Basel, Switzerland. This article is an open access article distributed under the terms and conditions of the Creative Commons Attribution (CC BY) license (<https://creativecommons.org/licenses/by/4.0/>).

1. Introduction

Noncircular gear is a mechanism that can realize the non-uniform speed ratio transmission between the driving gear and driven gear [1]. It is widely used in agriculture, textile, instruments, and other fields because of its advantages of low economic cost, compact structure, accurate transmission ratio, high efficiency, strong bearing capacity, and high precision. In the 14th century, high precision noncircular gear mechanism began to be used in astronomical clocks [2]. After the 20th century, many scholars have carried out the research on noncircular gear and made great progress in related design theory and engineering application.

Litvin et al. [1] carried out systematic research on the design and manufacture of noncircular gear. Liu et al. [3] studied the application of a noncircular gear train in the generation of specific trajectory curve. Mundo et al. [4,5] studied the tooth surface design method, motion characteristics, and application occasions of noncircular gear planetary transmission, as well as the noncircular gear five-link mechanism, and optimized the connecting rod curve of the traditional five-link mechanism based on the noncircular gear. Ottaviano et al. [6] studied the kinematic characteristics of noncircular gear and cam function generator through numerical calculation and experimental analysis. Modler et al. [7]

made a comprehensive analysis on the mechanism of noncircular gear linkage, including the types and mechanical characteristics of noncircular gear linkage, which laid a theoretical foundation for its application. Alexandru et al. [8] deeply studied the characteristics and geometric design method of variable transmission ratio steering gear. Zheng et al. [9] combined the principle of noncircular gear differential gear train and the motion requirements of indexing device and proposed a new noncircular gear indexing device. This device has the characteristics of large indexing of a planetary indexing cam mechanism, more compact structure, and fewer parts. Yu et al. [10] carried out simulation and experimental research on the surface topography and machining surface quality of noncircular gear in ball end milling. Based on the research of plane noncircular gear, Lin and Gong et al. [11] creatively proposed a new type of curve face gear pair, which can realize the variable transmission ratio transmission between intersecting shafts, and analyzed its principle and motion characteristics. Lin and Zeng et al. [12] analyzed the design and tooth width characteristics of helical curve face gear pair. Lin and Yu et al. [13,14] studied the composite motion characteristics and bending stress of high-speed curve face gear pair. Hu et al. [15] studied the mathematical model of curve face gear and time-varying meshing characteristics of compound transmission, and found that this gear pair can be used for the focusing mechanism.

In the field of gear CVT, there have been a few studies. Dooner et al. [16] proposed a noncircular gear CVT device based on the summation differential principle, and dealt with its kinematic characteristics and circulating power. Sun et al. [17] proposed a heart-shaped gear CVT device based on the principle of noncircular gear variable transmission ratio, and introduced its mathematic model and kinematic characteristics. According to the crank slider principle and eccentric cam principle, Zhu and Wang proposed a gear infinitely variable transmission with control function [18,19] and a novel gear infinitely variable transmission based on the scotch yoke systems [20]. They can be applied to vehicle and wind turbine, and the simulation and experimental analysis were carried out. Chen et al. [21] proposed a new rod gear pulse CVT and analyzed its transmission characteristics and phase number optimization. Compared with the other traditional CVT, it has a wider variable range of transmission ratio and smaller pulsation rate while reducing volume.

The above mechanisms can realize CVT in a certain sense, but there is still some room for improvement in the overall transmission characteristics and meshing performance, like transmission type, mechanism volume, design difficulty, kinematic characteristics, transmission efficiency and bearing capacity. In order to improve the above performance, according to the transmission ratio integration method consisting of addition method and multiplication method, the spatial noncircular gear CVT was proposed. Here, noncircular gear pair and curve face gear pair are collectively referred to as spatial noncircular gear pair. Firstly, in terms of transmission type and mechanism volume, the spatial noncircular gear CVT contains multiple transmission patterns. According to the requirements of different working conditions, different spatial noncircular gear CVT pattern can be selected. In addition, for design difficulty and mechanism kinematic characteristics, the spatial noncircular gear CVT mechanism combined the characteristics of a spatial noncircular gear pair, a transmission ratio changing mechanism, a transmission selection mechanism, and multiple branches. It can dynamically adjust the design parameters according to the actual transmission ratio requirements to realize the CVT with the input rotation angle in the whole range. Based on the tooth profile classification design method, the spatial noncircular gear with different tooth profiles can be obtained. Finally, compared with other transmission forms, spatial noncircular gear transmission, as a meshing transmission form, has high bearing capacity and transmission efficiency. In summary, this study can provide a new idea for vehicles and special vehicles with special transmission needs to realize CVT.

In this paper, the pattern classification and design, transmission principle, and simulation of spatial noncircular gear CVT pattern were carried out. The pitch curve, tooth surface classification design, and transmission experiment of curve face gear pairs with different

tooth profiles were introduced in detail. The correctness of the pattern classification and design of spatial noncircular gear CVT was verified, with the hope of creating a certain foundation for further research and for the application of spatial noncircular gear CVT. The research process was shown in Figure 1.

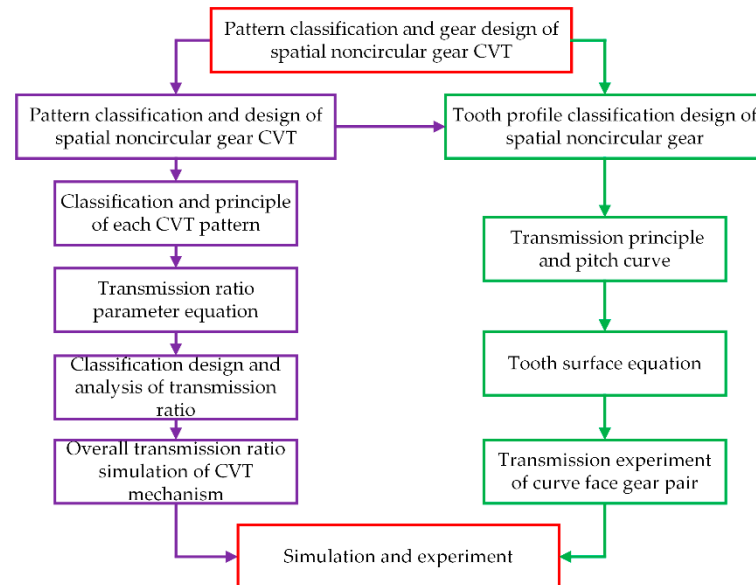


Figure 1. Research workflow of spatial noncircular gear CVT.

2. Pattern Classification of Spatial Noncircular Gear CVT

Spatial noncircular gear CVT pattern can be divided into two categories, with a total of five subcategories, as shown in Table 1 and Figure 2. Type I is the addition method, including classes A, B, and C, named NG-PBGT, NG-PCGT, and CFG-BG-PCGT, respectively. Type II is the multiplication method, including classes D and E, named CFG and NG, respectively.

Table 1. CVT pattern of spatial noncircular gear.

Type	I: Addition Method			II: Multiplication Method	
	Class A	Class B	Class C	Class D	Class E
Name	NG-PBGT	NG-PCGT	CFG-BG-PCGT	CFG	NG
Transmission ratio changing mechanism	Noncircular gear pair and planetary bevel gear train	Noncircular gear pair and planetary cylindrical gear train	Curve face gear pair, bevel gear pair and planetary cylindrical gear train	Curve face gear pair	Noncircular gear pair

In Figure 2, ω_i and ω_o are the input and output angular velocities, respectively. The spatial noncircular gear CVT mechanism includes three parts. The first part is the phase switching mechanism, which is responsible for adjusting the phase angle between the two driving spatial noncircular gears and synchronizing their rotation speed at the same time. The second part is the transmission ratio changing part, which is responsible for integrating the transmitted variable transmission ratio to achieve a constant speed output within a certain range of input rotation angle. The third part is the transmission selection mechanism, which is responsible for selecting the transmission ratio transmitted in order to only output a constant rotation speed during the transmission. Through the transmission selection mechanisms of multiple branches, the transmission ratio of each branch at different input rotation angles was integrated, and finally a constant rotation speed output with the input rotation angle in the range of 0 to 360° was realized.

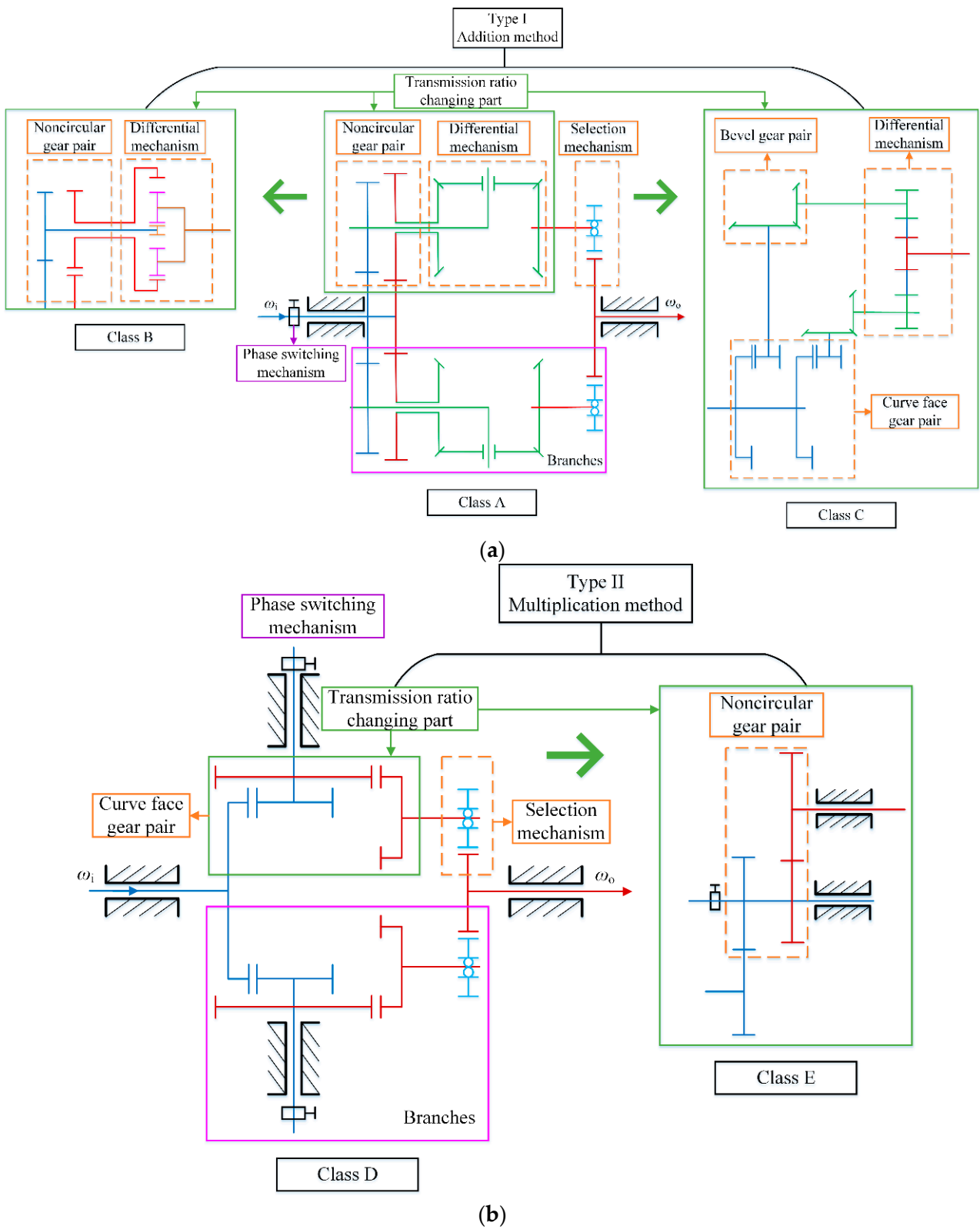


Figure 2. CVT pattern of spatial noncircular gear. (a) Type I: Addition method. (b) Type II: Multiplication method.

The structure of the phase switching mechanism and the transmission selection mechanism of the five patterns are the same, but the transmission ratio changing part is different. For the three classes included in type I, the transmission ratio changing part is composed

of different spatial noncircular gear mechanisms and differential mechanisms. Through the addition method, the transmission ratios of gear pairs were integrated to achieve a constant speed output. For the two classes included in type II, the transmission ratio changing part is composed of different spatial noncircular gear mechanisms. Through the multiplication method, the transmission ratios of gear pairs were integrated to achieve a constant speed output. The structural composition of the transmission ratio changing part of each pattern is shown in Table 1.

3. Principle and Classification Design of Spatial Noncircular Gear CVT

3.1. Principle of Each CVT Pattern

The principles of the five CVT patterns are described in detail later. The phase switching mechanism and transmission selection mechanism are applicable to the five patterns, so only class A was taken as an example to explain them.

(1) Class A: NG-PBGT

Figure 3 shows the transmission principle of class A.

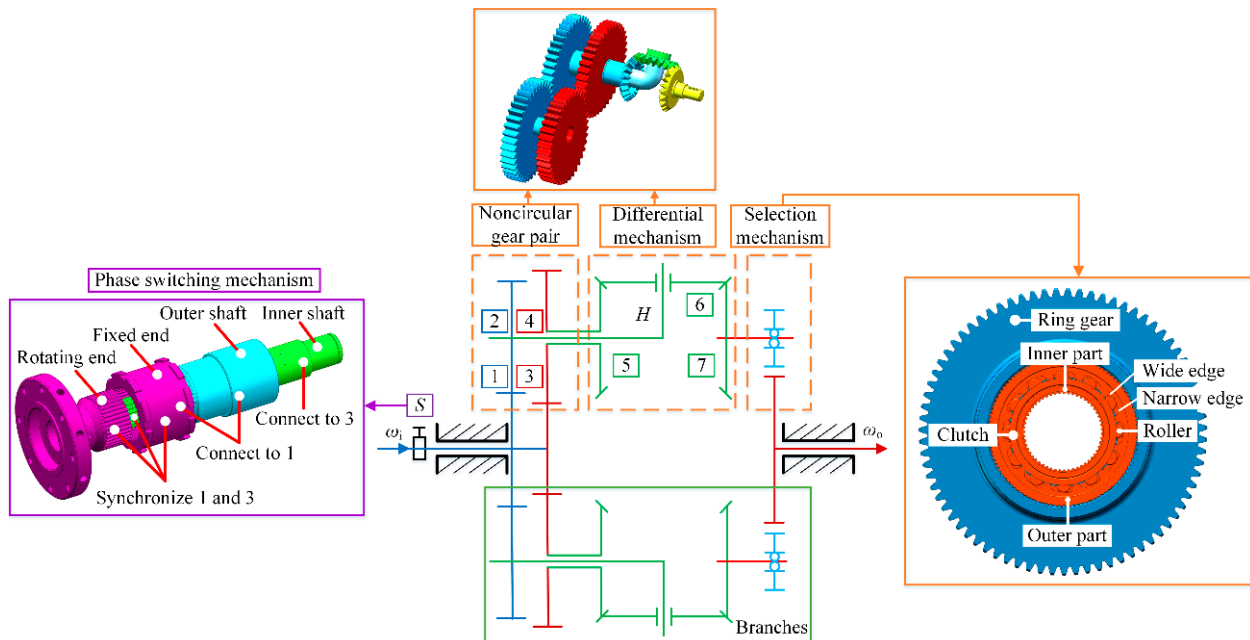


Figure 3. Transmission principle of class A.

This mechanism includes four parts. The first part is the phase switching mechanism, which is composed of a rotating end, a fixed end, an outer shaft, and an inner shaft. The outer shaft is connected with the fixed end and the noncircular gear 1 at the same time, and the inner shaft is connected with the rotating end and the noncircular gears 3 at the same time. Step 1, by rotating the rotating end, there is a required phase angle between noncircular gears 1 and 3. Step 2, connect the rotating end with the fixed end to synchronize the rotation speed of noncircular gears 1 and 3. In steps 1 and 2, the phase angle was switched. The second part is the noncircular gear pair, which is responsible for generating the required variable transmission ratio. The third part is the differential mechanism, which is composed of a planetary bevel gear train. It is responsible for integrating the variable transmission ratios of the driven noncircular gears 2 and 4 to achieve a constant speed output within a certain range of input rotation angle. The fourth part is the transmission selection mechanism, which is composed of a clutch and a ring gear. The outer ring of the clutch is connected to the inside of the ring gear, and the outside of the ring gear is connected to the output end. The clutch only transmits one-way rotational motion. When the inner ring of the clutch rotates in one direction, the roller was driven to roll to the narrow side of the wedge groove to be clamped with the outer ring of the clutch, thereby

driving the outer ring of the clutch to rotate. When the inner ring of the clutch rotates in reverse, the roller rolls to the wide edge of the wedge groove and is in a relaxed state with the outer ring of the clutch, resulting in the outer ring of the clutch not rotating. This branch does not transfer rotation at this time. By integrating the transmission ratios of multiple branches, the constant speed output with the input rotation angle in the range of 0 to 360° was realized. The CVT can be realized by continuously changing the phase angle.

In brief, the rotation speed transmission process of class A is as follows. Step 1, the input rotation speed was transmitted to the noncircular gears 1 and 3 with a certain phase angle. Step 2, the planetary bevel gear train composed of the bevel gears 5, 6, and 7 integrated the variable rotation speeds of noncircular gears 2 and 4. Step 3, the bevel gear 7 outputted a constant rotation speed within a certain input rotation angle. The planet carrier H is connected to the noncircular gear 2, and the bevel gear 5 is connected to the noncircular gear 4.

(2) Class B: NG-PCGT

Figure 4 is the transmission principle of class B, and the transmission process is as follows. Step 1, the input rotation speed was transmitted to the noncircular gears 1 and 3 with a certain phase angle. Step 2, the planetary cylindrical gear train composed of the ring gear 5, planetary gear 6, and center gear 7 integrated the variable rotation speeds of noncircular gears 2 and 4. Step 3, the planetary carrier H outputted a constant rotation speed within a certain input rotation angle. The ring gear 5 is connected to the noncircular gear 4, and the center gear 7 is connected to the noncircular gear 2.

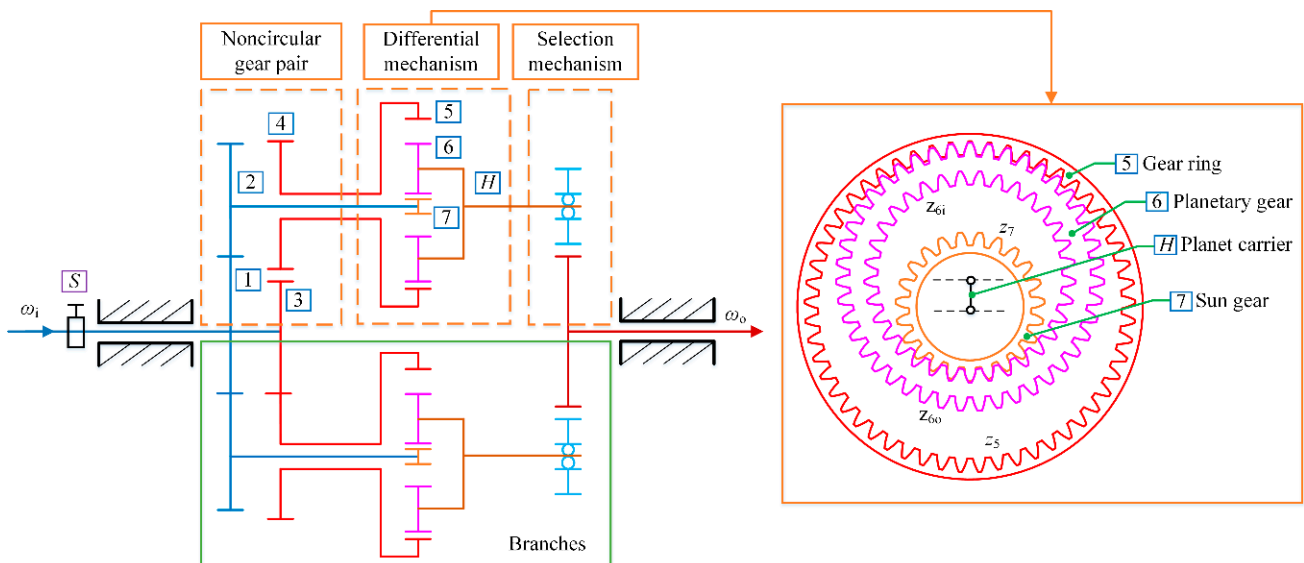


Figure 4. Transmission principle of class B.

(3) Class C: CFG-BG-PCGT

Figure 5 is the transmission principle of class C. The transmission process is as follows. Step 1, the input rotation speed was transmitted to the curve face gears 1 and 3 with a certain phase angle. Step 2, two pairs of bevel gear pairs adjusted the variable rotation speed of noncircular gears 2 and 4 and changed their directions, respectively. Step 3, the planetary cylindrical gear train consisting of the cylindrical gears 9, 11, and 13 and the bilateral gears 10 and 12 integrated the rotational speeds of the bevel gears 6 and 8. Step 4, the planetary carrier H outputted a constant rotation speed within a certain input rotation angle. The gear 9 is connected to the bevel gear 6, and the gear 13 is connected to the bevel gear 8.

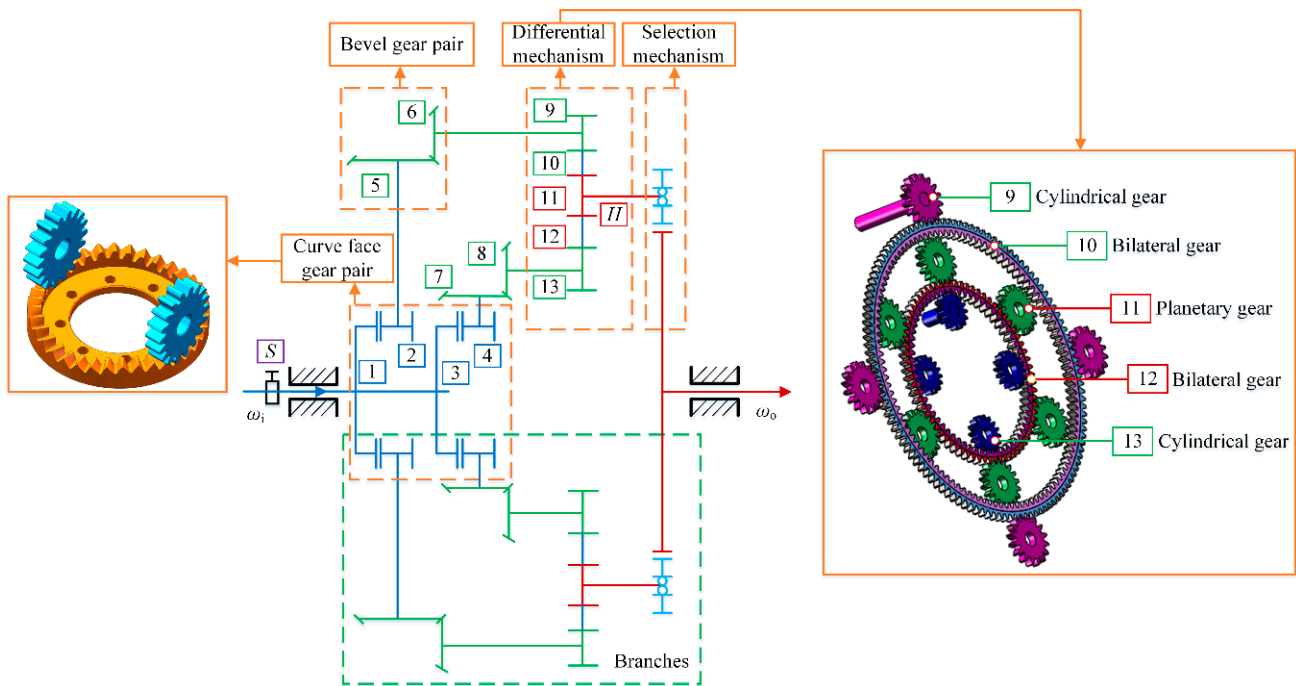


Figure 5. Transmission principle of class C.

(4) Class D: CFG and class E: NG

For classes D and E, the transmission principle is the same, but the difference lies in the different types of gear pairs. Figure 6 is the transmission principle of classes D and E. In Figure 6a, both gear pairs are curve face gear pairs. In Figure 6b, both gear pairs are noncircular gear pairs. The transmission process is as follows. Step 1, the input rotation speed was transmitted to gear 2. Step 2, gears 1 and 3 with a phase angle integrated the variable rotation speed. Step 3, gear 4 outputted a constant rotation speed within a certain input rotation angle.

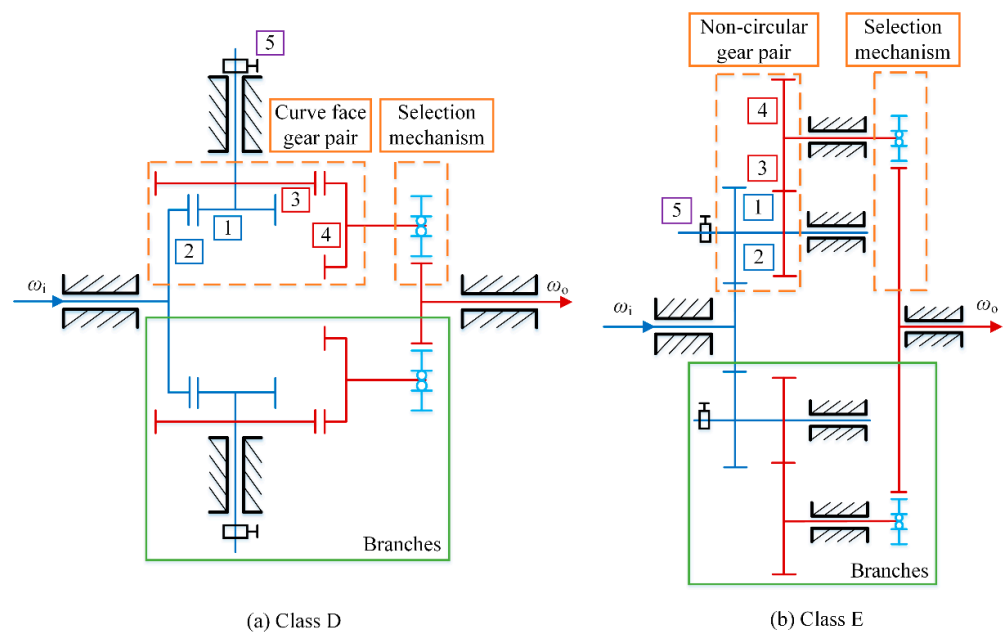


Figure 6. Transmission principle of classes D and E.

3.2. Transmission Ratio Parameter Equation

According to the analysis in Section 3.1, the transmission ratio parameter equations of spatial noncircular gear pairs were designed, respectively, and the intermediate transmission ratio and overall transmission ratio of each pattern were calculated. See Table 2 for each parameter equation.

Table 2. Transmission ratio parameter equation of each CVT pattern.

Type	Class	Transmission Ratio	Characteristic Parameter
I	A	$\begin{cases} i_{21} = -(a_1\theta_1 + b_1) \\ i_{43} = -(a_2\theta_3 + b_2) \\ i_{7i} = Ki_{43} + (1 - K)i_{21} \\ i_{oi} = i_{7i}i_{o7} = -\{[Ka_2 + (1 - K)a_1]\theta_1 + Ka_2\theta_p + Kb_2 + (1 - K)b_1\}i_{o7} \end{cases}$	$K = -\frac{z_6}{z_7} \times \frac{z_5}{z_6}$
	B	$\begin{cases} i_{21} = -(a_1\theta_1 + b_1) \\ i_{43} = -(a_2\theta_3 + b_2) \\ i_{Hi} = \frac{Ki_{43} - i_{21}}{K - 1} \\ i_{oi} = i_{Hi}i_{oH} = -\frac{(Ka_2 - a_1)\theta_1 + Ka_2\theta_p + Kb_2 - b_1}{K - 1}i_{oH} \end{cases}$	$K = \frac{z_{6i}}{z_7} \times \frac{z_5}{z_{6o}}$
	C	$\begin{cases} i_{21} = a_1\theta_1 + b_1 \\ i_{43} = a_2\theta_3 + b_2 \\ i_{Hi} = \frac{Ki_{21} - i_{43}}{K - 1} \\ i_{oi} = i_{Hi}i_{oH} = \frac{(Ka_1 - a_2)\theta_1 - a_2\theta_p + Kb_1 - b_2}{K - 1}i_{oH} \end{cases}$	$K = \frac{z_{12i} z_{11} z_{10i} z_9}{z_{13} z_{12o} z_{11} z_{10o}}$
II	D	$\begin{cases} i_{21} = a^{\theta_1} \\ i_{43} = a^{\theta_3} \\ i_{oi} = i_{42}i_{o4} = -a^{\theta_p}i_{o4} \end{cases}$	/
	E	$\begin{cases} i_{21} = -a^{\theta_1} \\ i_{43} = -a^{\theta_3} \\ i_{oi} = i_{42}i_{o4} = a^{\theta_p}i_{o4} \end{cases}$	

In Table 2, θ_1 and $\theta_3 = \theta_1 + \theta_p$ are the rotation angles of gears 1 and 3 under each pattern, respectively. θ_p is the phase angle. i_{21} and i_{43} are the transmission ratios of the corresponding gear pairs, respectively. i_{oi} is the overall transmission ratio between the output shaft and input shaft. $a_1, b_1, a_2,$ and b_2 are the parameters of the transmission ratios i_{21} and i_{43} of type I. K is the characteristic parameter of the differential mechanism of type I. a is the parameter of the transmission ratios i_{21} and i_{43} of type II.

For class A, $z_5, z_6,$ and z_7 are the teeth number of bevel gears 5, 6, and 7, respectively. i_{7i} is the transmission ratio between the bevel gear 7 and the input shaft. Constant i_{o7} is the transmission ratio between the output shaft and the bevel gear 7. For class B, z_5 and z_7 are the teeth number of the ring gear 5 and center gear 7, respectively. z_{6i} and z_{6o} are the number of internal teeth and external teeth of planetary gear 6, respectively. i_{Hi} is the transmission ratio between the planet carrier H and input shaft. Constant i_{oH} is the transmission ratio between the output shaft and the planet carrier H . For class C, $z_9, z_{11},$ and z_{13} are the teeth number of the corresponding gears, respectively. $z_{10i}, z_{10o}, z_{12i},$ and z_{12o} are the teeth number of the inner and outer rings of the corresponding bilateral gears. i_{Hi} is the transmission ratio between the planet carrier H and input shaft. Constant i_{oH} is the transmission ratio between the output shaft and the planet carrier H . For classes D and E, i_{42} is the transmission ratio between gear 4 and gear 2. Constant i_{o4} is the transmission ratio between the output shaft and gear 4.

As can be seen from Table 2, when the coefficient related to the rotation angle θ_1 is 0, the overall transmission ratio i_{oi} of each pattern is a function related only to the variable phase angle θ_p . By continuously changing θ_p , combined with the transmission selection mechanisms of multiple branches, the CVT with an input rotation angle in the range of 0 to 360° can be realized. The parameter conditions that each pattern need to meet were shown in Table 3.

Table 3. Parameter conditions for each pattern.

Class	Parameter Condition
A	$Ka_2 + (1-K)a_1 = 0, Ka_2 \neq 0$
B	$Ka_2 - a_1 = 0, Ka_2 \neq 0, K \neq 1$
C	$Ka_1 - a_2 = 0, a_2 \neq 0, K \neq 1$
D	
E	$a > 0, a \neq 1$

3.3. Classification Design and Analysis of Transmission Ratio

The transmission ratio of spatial noncircular gear pair in Table 2 is the transmission ratio of the working area where motion and power are transmitted. In order to obtain a complete transmission ratio, a polynomial method can be used to construct the transmission ratio function of the transition area where only motion is transmitted but no power is transmitted, and the periodic transmission ratio was obtained. Taking noncircular gears 1 and 2 as examples, the transmission ratio equation is shown in Equation (1), and the transmission ratios of other spatial noncircular gear pairs can be obtained in the same way.

$$i_{21}(\theta_1) = \begin{cases} i_{01}(\theta_1), \theta_1 \in [0, \Phi] \\ i_{02}(\theta_1) = \sum_{j=0}^6 (m_j \theta_1^j), \theta_1 \in [\Phi, U] \end{cases} \quad (1)$$

where, $i_{01}(\theta_1)$ is the transmission ratio in the working area. $i_{02}(\theta_1)$ is the transmission ratio in the transition area. m_j is the polynomial coefficient. Φ is the maximum rotation angle of noncircular gear 1 in the working area. $U = 2\pi/n_1$ is the period of the transmission ratio, and the positive integer n_1 is the order of noncircular gear 1.

According to Equation (2), the unknown parameters in $i_{21}(\theta_1)$ can be solved.

$$\begin{cases} \frac{2\pi}{n_2} = \int_0^\Phi i_{01}(\theta_1) d\theta_1 + \int_\Phi^U i_{02}(\theta_1) d\theta_1 \\ i_{01}(\Phi) = i_{02}(\Phi) \\ i'_{01}(\Phi) = i'_{02}(\Phi) \\ i''_{01}(\Phi) = i''_{02}(\Phi) \\ i_{01}(0) = i_{02}(U) \\ i'_{01}(0) = i'_{02}(U) \\ i''_{01}(0) = i''_{02}(U) \end{cases} \quad (2)$$

where the positive integer n_2 is the order of noncircular gear 2. $i'_{01}(\theta_1)$, $i''_{01}(\theta_1)$, $i'_{02}(\theta_1)$, and $i''_{02}(\theta_1)$ are the first and second derivatives of $i_{01}(\theta_1)$ and $i_{02}(\theta_1)$ with respect to θ_1 , respectively.

According to the above analysis, take the parameters in Table 4 and analyze the transmission ratio of each pattern, as shown in Figures 7 and 8. n_i is the number of cycles of the input gear and n_l is the number of branches.

Table 4. Structural parameters of each pattern.

Parameters	Φ/Rad	a_1	b_1	a_2	b_2	θ_p / rad	K	n_i	n_l	a	n_1	n_2
Class A	11π/9	0.09	0.9	0.24	0.45	π/6	-0.6	1	3		1	1
Class B		0.24	0.46	0.12	0.23		2	1	3	/	1	1
Class C	5π/9	0.30	1.7	0.48	0.8	π/18	1.6	2	2		2	1
Class D	11π/18							2	3	1.03	2	2
Class E	10π/9		/			π/6	/	1	3	1.04	1	1

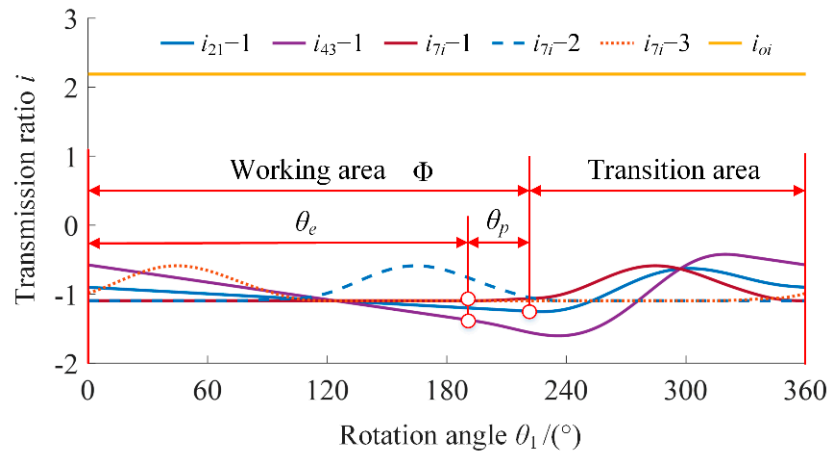


Figure 7. Transmission ratio variation law of class A.

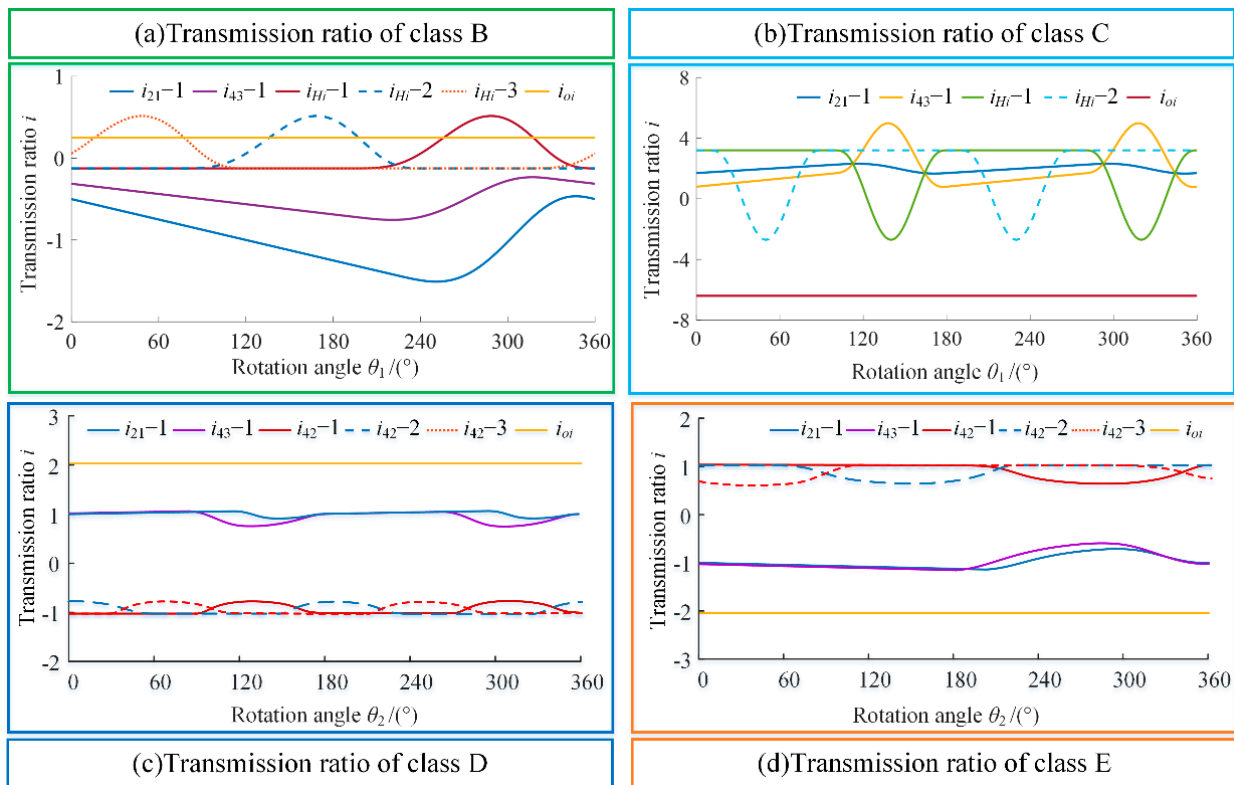


Figure 8. Transmission ratio variation law of class B~E.

Figure 7 is the variation law of the transmission ratio of class A. $\theta_e = \Phi - \theta_p$ is the length of the effective working area, that is, the area where each branch outputs a constant rotation speed. To achieve a constant rotation speed output with an input rotation angle in the range of 0 to 360°, Equation (3) must be satisfied.

$$\theta_e \geq \theta_{emin}, \tag{3}$$

where $\theta_{emin} = 2\pi/(n_i \cdot n_1)$ is the minimum length of the effective working area.

In Figure 7, i_{21-1} , and i_{43-1} are the transmission ratios of the corresponding gear pairs in the first branch, respectively. i_{7i-1} , i_{7i-2} , and i_{7i-3} are the transmission ratios between the bevel gear 7 and the input shaft in the three branches, respectively. Here, Φ is 220°, θ_p is 30° and θ_e is 190°. As can be seen, by integrating the transmission ratios i_{21} and i_{43} in the three branches, respectively, i_{7i-1} , i_{7i-2} , and i_{7i-3} are constant in a certain area. Specifically,

i_{7i-1} is constant when θ_1 varies from 0 to 190° . i_{7i-2} is constant when θ_1 varies in the range $0\sim 70^\circ$ and $240\sim 360^\circ$. i_{7i-3} is constant when θ_1 varies in the range $120\sim 310^\circ$. Finally, by integrating the transmission ratios i_{7-1} , i_{7i-2} , and i_{7i-3} , the overall transmission ratio i_{oi} is always constant when θ_1 varies from 0 to 360° .

Figure 8 shows the variation law of the transmission ratios of classes B~E.

In Figure 8, i_{21-1} , and i_{43-1} are the transmission ratios of the corresponding gear pairs in the first branch, respectively. i_{oi} is the overall transmission ratio between the output shaft and input shaft. In Figure 8a,b, the input rotation angle is θ_1 . i_{Hi-1} , i_{Hi-2} , and i_{Hi-3} are the transmission ratios between the planet carrier H and input shaft in each branch, respectively. In Figure 8c,d, the input rotation angle is θ_2 . i_{42-1} , i_{42-2} , and i_{42-3} are the transmission ratios between gear 4 and gear 2 in the three branches, respectively. Similarly, the maximum working angle Φ of class B~E are 220° , 100° , 110° , and 200° . The phase angle θ_p of class B~E are 30° , 10° , 30° , and 30° . The length of the effective working area θ_e of class B~E are 190° , 90° , 80° , and 170° . By integrating the transmission ratios i_{21} and i_{43} of each branch, respectively, i_{Hi} and i_{42} of each branch are constant in a certain area. Finally, through the integration of the transmission ratios of multiple branches, each pattern can achieve a constant rotation speed output throughout the area. CVT can be realized by continuously changing the phase angle.

4. Tooth Profile Classification Design of Spatial Noncircular Gear

The design of the noncircular gear pair has been relatively mature, and the tooth profile design can be referred to [1]. However, the tooth surfaces of curve face gear pairs with different tooth profiles are more complicated and need to be analyzed in detail. The tooth profile of the curve face gear pair includes straight tooth, helical tooth, and curvilinear tooth, as shown in Figure 9. Compared with the straight tooth curve face gear pairs, the helical tooth and curvilinear tooth curve face gear pairs have a more complicated design process, but have a larger contact ratio and load-bearing capacity, which can meet the needs of different working conditions. Therefore, it is necessary to carry out the tooth profile classification design of curve face gear pair.

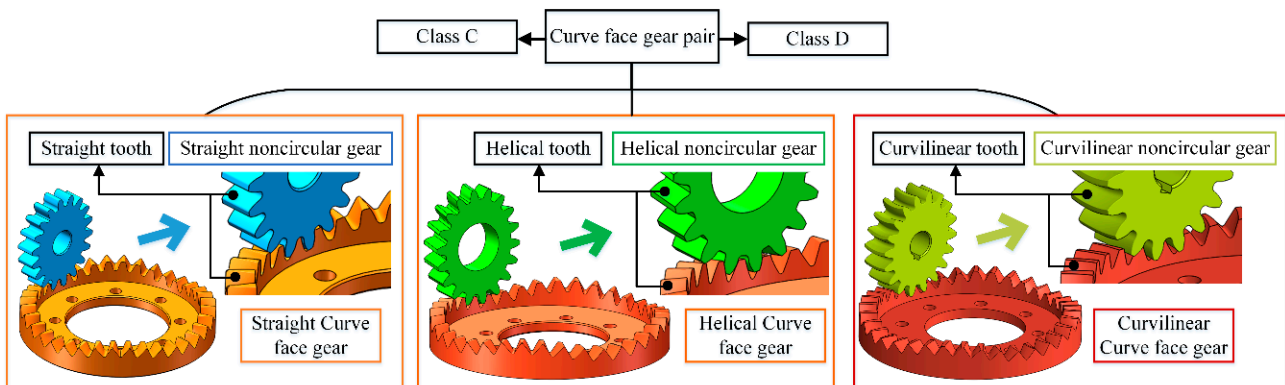


Figure 9. Tooth profile classification of curve face gear pair.

4.1. Transmission Principle and Pitch Curve

According to the gear meshing principle, the pitch curve of the curve face gear pair is independent of the tooth profile. Figure 10 is the meshing coordinate system of the pitch curve of the curved face gear pair. σ_1 and σ_2 are the corresponding pitch curves, respectively. ω_1 and ω_2 are the corresponding angular velocities, respectively. The coordinate system S_f ($O_f-X_fY_fZ_f$), abbreviated as S_f , is the fixed coordinate system of the noncircular gear frame. The coordinate system S_1 ($O_1-X_1Y_1Z_1$), abbreviated as S_1 , is the follow-up coordinate system of the noncircular gear. The coordinate system S_m ($O_m-X_mY_mZ_m$), abbreviated as S_m , is the fixed coordinate system of the curve face gear frame. The coordinate system S_2 ($O_2-X_2Y_2Z_2$), abbreviated as S_2 , is the follow-up coordinate system of the curve face gear.

When the gear pair is in the initial meshing situation A, S_1 and S_f coincide and S_2 and S_m coincide. When the gear pair changes from situation A to situation B, the rotation axes Z_1 and Z_2 of the two gears are fixed, and the meshing point of the pitch curve changes from P_1 to P_2 . θ_1 and θ_2 are the rotation angles of the noncircular gear and curve face gear respectively. $r_1(\theta_1)$ and $r_2(\theta_2)$ are the pitch curve parameter equation of the noncircular gear and curve face gear, respectively. R is the distance from the projection of point P_1 on the pitch curve of curve face gear in plane $X_m O_m Y_m$ to O_2 . V_1 and V_2 are the speeds at the meshing points of the two curves, respectively.

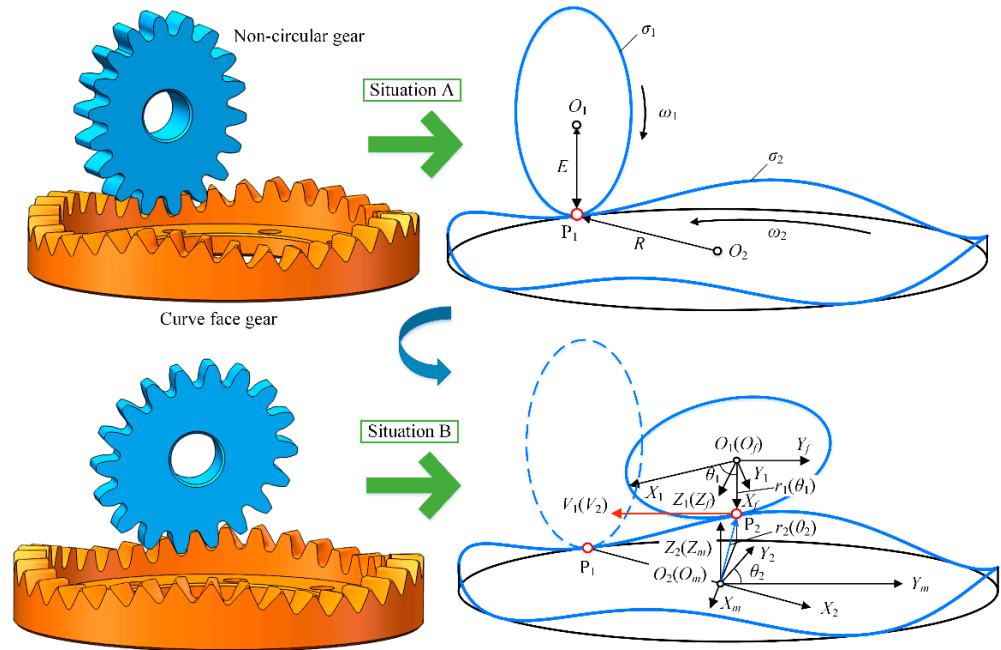


Figure 10. Pitch curve coordinate system of the curve face gear pair.

According to the principle of spatial coordinate transformation, the homogeneous transformation matrix from the coordinate system S_1 to S_f is

$$M_{f1} = \begin{bmatrix} \cos \theta_1 & \sin \theta_1 & 0 & 0 \\ -\sin \theta_1 & \cos \theta_1 & 0 & 0 \\ 0 & 0 & 1 & 0 \\ 0 & 0 & 0 & 1 \end{bmatrix}. \tag{4}$$

The homogeneous transformation matrix from the coordinate system S_f to S_m is

$$M_{mf} = \begin{bmatrix} 0 & 0 & 1 & -R \\ 0 & 1 & 0 & 0 \\ -1 & 0 & 0 & E \\ 0 & 0 & 0 & 1 \end{bmatrix}. \tag{5}$$

The homogeneous transformation matrix from the coordinate system S_m to S_2 is

$$M_{2m} = \begin{bmatrix} \cos \theta_2 & \sin \theta_2 & 0 & 0 \\ -\sin \theta_2 & \cos \theta_2 & 0 & 0 \\ 0 & 0 & 1 & 0 \\ 0 & 0 & 0 & 1 \end{bmatrix}. \tag{6}$$

Then, the homogeneous transformation matrix from the coordinate system S_1 to S_2 can be expressed as

$$M_{21} = M_{2m}M_{mf}M_{f1} = \begin{bmatrix} -\sin \theta_1 \sin \theta_2 & \cos \theta_1 \sin \theta_2 & \cos \theta_2 & -R \cos \theta_2 \\ -\cos \theta_2 \sin \theta_1 & \cos \theta_1 \cos \theta_2 & -\sin \theta_2 & R \sin \theta_2 \\ -\cos \theta_1 & -\sin \theta_1 & 0 & E \\ 0 & 0 & 0 & 1 \end{bmatrix}. \quad (7)$$

The coordinates of point P_2 in S_1 are $[r_1(\theta_1)\cos(\theta_1), r_1(\theta_1)\sin(\theta_1), 0, 1]^T$, then the coordinates of point P_2 in S_2 can be expressed as

$$\begin{bmatrix} x_2 \\ y_2 \\ z_2 \\ 1 \end{bmatrix} = M_{21} \begin{bmatrix} r_1(\theta_1) \cos \theta_1 \\ r_1(\theta_1) \sin \theta_1 \\ 0 \\ 1 \end{bmatrix} = \begin{bmatrix} -R \cos \theta_2 \\ R \sin \theta_2 \\ E - r_1(\theta_1) \\ 1 \end{bmatrix}. \quad (8)$$

Therefore, the pitch curve equation of the curve face gear can be obtained as

$$\begin{cases} x_2 = -R \cos \theta_2 \\ y_2 = R \sin \theta_2 \\ z_2 = E - r_1(\theta_1) \end{cases}. \quad (9)$$

It can be seen from Equation (9) that the pitch curve of the curve face gear is a cylindrical curve with R as the radius.

The speeds V_1 and V_2 satisfy Equation (10).

$$\begin{cases} V_1 = r_1(\theta_1)\omega_1 \\ V_2 = R\omega_2 \\ V_1 = V_2 \end{cases}. \quad (10)$$

Then, the transmission ratio of this gear pair is

$$i_{21}(\theta_1) = \frac{\omega_2}{\omega_1} = \frac{r_1(\theta_1)}{R}. \quad (11)$$

4.2. Tooth Surface Equation

The accurate tooth surface model of the curve face gear pair was obtained by the method shown in Figure 11. Firstly, the tooth surface equation of the generating rack was derived, then the tooth surface equation of the generating gear was obtained, and finally the tooth surface equations of the noncircular gear and curve face gear were obtained.

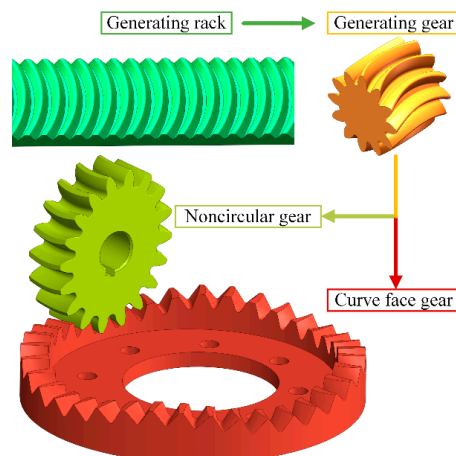


Figure 11. The tooth surface generating process of curve face gear pair.

(1) Tooth surface equation of the generating rack

The tooth surface Σ_r of the generating rack includes straight tooth, helical tooth, and curvilinear tooth. Figure 12 is the tooth surface coordinate system when the tooth profile is a helical tooth or curvilinear tooth. When the helix angle β_r is 0, it is a straight tooth generating rack.

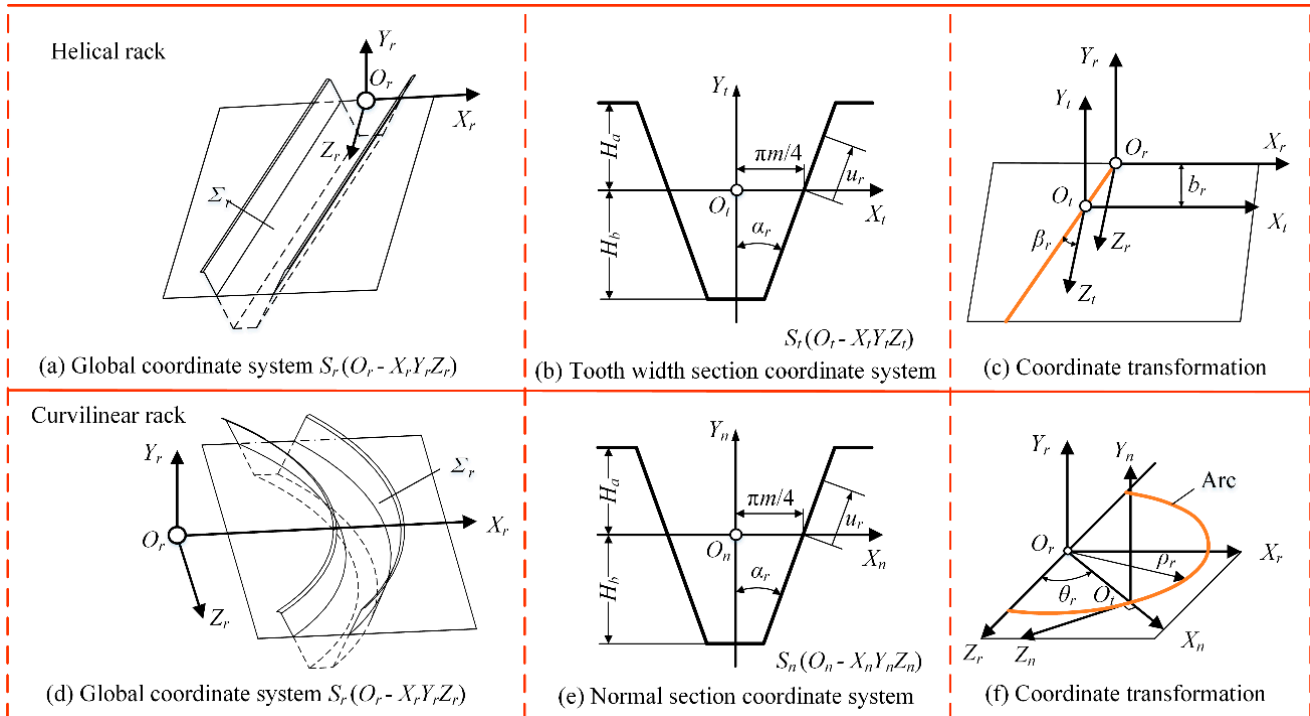


Figure 12. The tooth surface coordinate system of generating rack.

The global coordinate systems of both the helical and curvilinear tooth generating rack are expressed as $S_r(O_r-X_r Y_r Z_r)$, abbreviated as S_r , as shown in Figure 12a,d. In Figure 12b, $S_t(O_t-X_t Y_t Z_t)$, abbreviated as S_t , is the cross-section coordinate system of helical rack in the tooth width direction. $O_t X_t$ coincides with the rack pitch line and $O_t Y_t$ coincides with the cogging symmetry line. H_a and H_b are the addendum and dedendum, respectively. M is the module, α_r is the profile angle and u_r is the tooth height direction parameter. In Figure 12e, $S_n(O_n-X_n Y_n Z_n)$, abbreviated as S_n , is the normal section coordinate system of curvilinear rack. The normal section tooth profile of the curvilinear rack is the same as the cross-section tooth profile of the helical rack in the tooth width direction. Figure 12c,f show the transformation process from coordinate systems S_t and S_n to S_r , respectively. β_r and b_r are the helical angle and tooth width parameter of the helical rack respectively. θ_r and ρ_r are the arc angle and arc radius of the curvilinear rack, respectively. m is the module of the rack.

The tooth profile equations in S_t and S_n can be expressed as

$$r_t(u_r) = r_n(u_r) = \begin{bmatrix} \pm u_r \sin \alpha_r \pm \frac{\pi m}{4} \\ u_r \cos \alpha_r \\ 0 \\ 1 \end{bmatrix}, \tag{12}$$

where, the positive and negative signs, respectively, represent the left and right tooth surfaces of the rack.

The transformation matrices from S_t and S_n to S_r are

$$\begin{cases} \mathbf{M}_{rt}(b_r) = \begin{bmatrix} 1 & 0 & 0 & -b_r \tan \beta_r \\ 0 & 1 & 0 & 0 \\ 0 & 0 & 1 & b_r \\ 0 & 0 & 0 & 1 \end{bmatrix} \\ \mathbf{M}_{rn}(\theta_r) = \begin{bmatrix} \sin \theta_r & 0 & -\cos \theta_r & \rho_r \sin \theta_r \\ 0 & 1 & 0 & 0 \\ \cos \theta_r & 0 & \sin \theta_r & \rho_r \cos \theta_r \\ 0 & 0 & 0 & 1 \end{bmatrix} \end{cases} \quad (13)$$

Then, the tooth surface equations of the three kinds of tooth profiles in S_r can be expressed by $\mathbf{r}_r(u_r, b_r, \theta_r)$.

$$\mathbf{r}_r(u_r, b_r, \theta_r) = \begin{cases} \mathbf{r}_{r1}(u_r, b_r) = \mathbf{M}_{rt}(b_r)\mathbf{r}_t(u_r) \\ = [\pm u_r \sin \alpha_r \pm \frac{\pi m}{4} - b_r \tan \beta_r \quad u_r \cos \alpha_r \quad b_r \quad 1]^T \\ \mathbf{r}_{r2}(u_r, \theta_r) = \mathbf{M}_{rn}(\theta_r)\mathbf{r}_n(u_r) \\ = [(\pm u_r \sin \alpha_r \pm \frac{\pi m}{4}) \sin \theta_r + \rho_r \sin \theta_r \quad u_r \cos \alpha_r \quad (\pm u_r \sin \alpha_r \pm \frac{\pi m}{4}) \cos \theta_r + \rho_r \cos \theta_r \quad 1]^T \end{cases} \quad (14)$$

where $\mathbf{r}_{r1}(u_r, b_r)$ and $\mathbf{r}_{r2}(u_r, \theta_r)$ are the tooth surface equation of the helical rack and curvilinear rack, respectively. When $\beta_r = 0$, the tooth surface equation of the straight rack can be obtained by $\mathbf{r}_{r1}(u_r, b_r)$.

The three kinds of cylindrical generating gears have the same generation process. Through the envelope principle, the tooth surface of the generating gear can be obtained by the generating rack, as shown in Figure 13. The coordinate system S_r is fixed with the generating rack. The coordinate system $S_g (O_g-X_gY_gZ_g)$, abbreviated as S_g , is the fixed coordinate system of the generating gear frame. The coordinate system $S_c (O_c-X_cY_cZ_c)$, abbreviated as S_c , is the follow-up coordinate system of the generating gear. r_c is the radius of the generating gear. When the rotation angle of the generating gear is φ , the displacement distance of the generating rack is $r_c\varphi$.

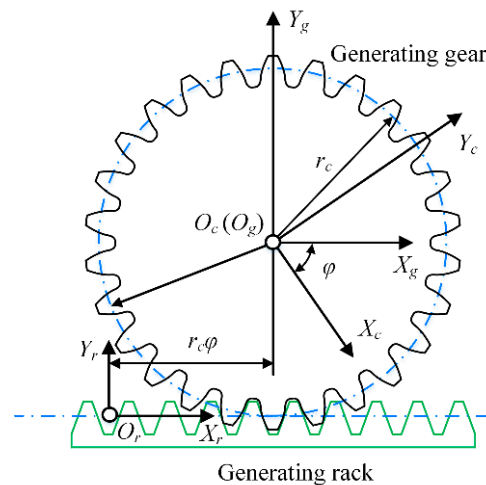


Figure 13. The generating process from the generating rack to cylindrical gear.

Based on the principle of spatial coordinate transformation, the transformation matrix from the coordinate system S_r to S_g is

$$\mathbf{M}_{gr} = \begin{bmatrix} 1 & 0 & 0 & -r_c\varphi \\ 0 & 1 & 0 & -r_c \\ 0 & 0 & 1 & 0 \\ 0 & 0 & 0 & 1 \end{bmatrix} \quad (15)$$

The transformation matrix from S_g to S_c is

$$M_{cg} = \begin{bmatrix} \cos \varphi & -\sin \varphi & 0 & 0 \\ \sin \varphi & \cos \varphi & 0 & 0 \\ 0 & 0 & 1 & 0 \\ 0 & 0 & 0 & 1 \end{bmatrix}. \tag{16}$$

Then, the transformation matrix from S_r to S_c can be expressed as

$$M_{cr} = M_{cg}M_{gr} = \begin{bmatrix} \cos \varphi & -\sin \varphi & 0 & -r_c(\varphi \cos \varphi - \sin \varphi) \\ \sin \varphi & \cos \varphi & 0 & -r_c(\varphi \sin \varphi + \cos \varphi) \\ 0 & 0 & 1 & 0 \\ 0 & 0 & 0 & 1 \end{bmatrix}. \tag{17}$$

The tooth surface equation of the generating gear in S_c can be expressed by $r_c(u_r, b_r, \theta_r)$.

$$r_c(u_r, b_r, \theta_r) = M_{cr}r_r(u_r, b_r, \theta_r). \tag{18}$$

Figure 14 is the generating process from the generating gear to the curve face gear pair. σ_c, σ_1 , and σ_2 are the pitch curve of the generating gear, noncircular gear, and curve face gear, respectively. When σ_1 is purely rolling around σ_2 , σ_c is purely rolling inside σ_1 . According to the relative motion relationship between σ_1 and σ_2 , the relative motion relationship between σ_c and σ_2 can be obtained.

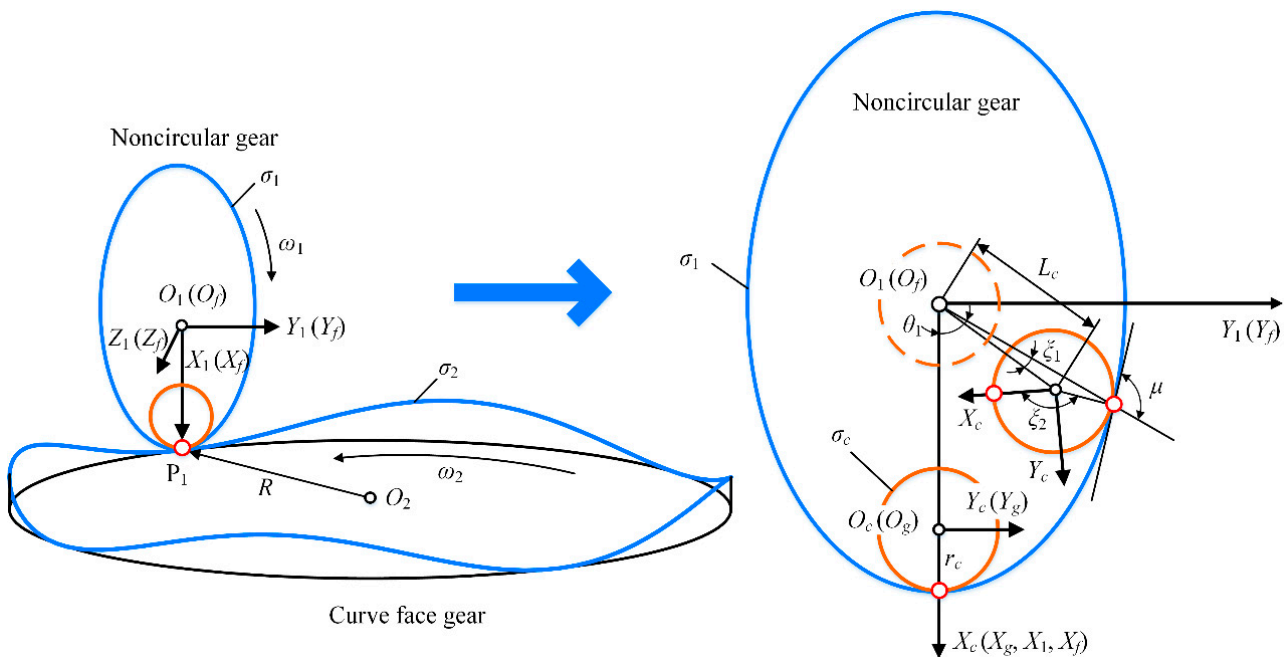


Figure 14. The generating process from the generating gear to the curve face gear pair.

The transformation matrix from the coordinate system S_c to S_1 is

$$M_{1c} = \begin{bmatrix} \cos \theta_c & \sin \theta_c & 0 & L_c \cos(\theta_1 - \xi_1) \\ -\sin \theta_c & \cos \theta_c & 0 & L_c \sin(\theta_1 - \xi_1) \\ 0 & 0 & 1 & 0 \\ 0 & 0 & 0 & 1 \end{bmatrix}, \tag{19}$$

where θ_c is the rotation angle of the generating gear around its own axis.

The expressions of the related parameters are as follows

$$\begin{cases} \xi_1 = \arccos \frac{r_1^2(\theta_1) + L_c^2 - r_c^2}{2r_1(\theta_1)L_c}, L_c = \sqrt{r_1^2(\theta_1) + r_c^2 - 2r_c r_1(\theta_1) \sin \mu} \\ \theta_c = \pi/2 + \xi_2 - \theta_1 - \mu, \xi_2 = \frac{\int_0^{\theta_1} \sqrt{r_1^2(\theta_1) + (dr_1(\theta_1)/d\theta_1)^2} d\theta_1}{r_c}, \mu = \arctan \frac{r_1(\theta_1)}{dr_1(\theta_1)/d\theta_1} \end{cases} \quad (20)$$

The transformation matrix from S_c to S_2 is

$$M_{2c} = M_{21}M_{1c} = \begin{bmatrix} -\sin \theta_2 \sin(\theta_c + \theta_1) & \sin \theta_2 \cos(\theta_c + \theta_1) & \cos \theta_2 & -R \cos \theta_2 - L_c \sin \theta_2 \sin \xi_1 \\ -\cos \theta_2 \sin(\theta_c + \theta_1) & \cos \theta_2 \cos(\theta_c + \theta_1) & -\sin \theta_2 & R \sin \theta_2 - L_c \cos \theta_2 \sin \xi_1 \\ -\cos(\theta_c + \theta_1) & -\sin(\theta_c + \theta_1) & 1 & E - L_c \cos \xi_1 \\ 0 & 0 & 0 & 1 \end{bmatrix} \quad (21)$$

Then, the tooth surface equation of the noncircular gear in S_1 can be expressed as

$$r_1(u_r, b_r, \theta_r, \theta_1) = M_{1c}(\theta_1)r_c(u_r, b_r, \theta_r). \quad (22)$$

The tooth surface equation of the curve face gear in S_2 can be expressed as

$$r_2(u_r, b_r, \theta_r, \theta_1) = M_{2c}(\theta_1)r_c(u_r, b_r, \theta_r). \quad (23)$$

By selecting the corresponding parameters, the tooth surfaces of the curve face gear pair with a straight, helical, and curvilinear tooth can be obtained, respectively. Combined with the transmission ratio equation in Section 3 and the tooth surface classification design, the 3D model of the curve face gear pair can be obtained.

5. Simulation and Experiment

Since the main difference between the five patterns is the transmission ratio changing part, and its complex key components are the curve face gear pair, the overall transmission ratio of each pattern was verified by simulation, and the transmission ratio of the curve face gear pair was verified by experiment.

5.1. Overall Transmission Ratio Simulation of CVT Mechanism

The mechanism models of five patterns were imported into the software ADAMS, and then the overall transmission ratios with different phase angles were simulated. Taking the phase angle in the range of 0 to 60° as an example, the comparison between the theoretical and simulation results was shown in Figure 15.

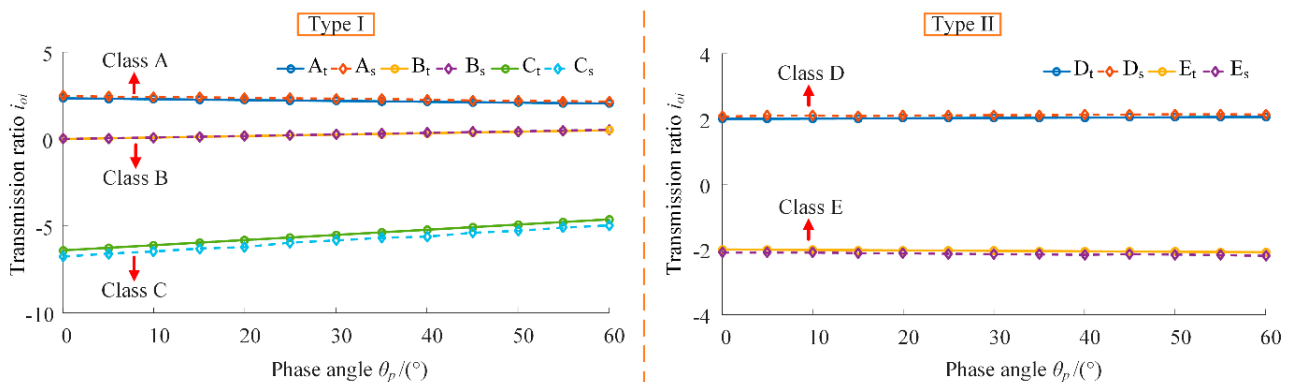


Figure 15. Comparison between theoretical and simulation results of overall transmission ratio.

In Figure 15, A_t , B_t , C_t , D_t , and E_t are the theoretical results of the overall transmission ratio of each pattern, respectively. A_s , B_s , C_s , D_s , and E_s are the simulation results of the overall transmission ratio. As can be seen, the overall transmission ratio values of classes A, B, and D are no less than 0, which means that the output shaft turns in the

same direction as the input shaft. The overall transmission ratio values of classes C and E are less than 0, which means that the output shaft turns in the opposite direction as the input shaft. Moreover, for classes A and C, the absolute values of i_{oi} gradually decrease with the increase of phase angle θ_p . For classes B, D, and E, the absolute values of i_{oi} gradually increase with the increase of phase angle θ_p . Further, for classes A, B, and C, the overall transmission ratio i_{oi} can be zero by selecting the appropriate parameters. At this time, no matter what the input rotation speed is, the output rotation speed is zero. However, for classes D and E, due to the limitation of transmission ratio principle, the overall transmission ratio i_{oi} cannot be zero. On the whole, the simulation results are in good agreement with the theoretical results, and the overall transmission ratio changes continuously with the continuous change of the phase angle, that is, the CVT was realized.

Figure 16 shows the maximum relative error of overall transmission ratio simulation for each pattern. For classes A~E, the maximum relative errors are 6.2%, 6.9%, 7.6%, 4.9%, and 5.4%. The reason why the error of type I is greater than that of type II is that the structure of type I mechanism is more complex, and the transmission chain is longer, resulting in greater transmission ratio loss and transmission ratio error.

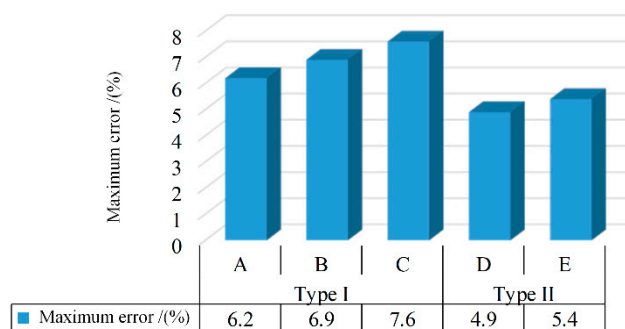


Figure 16. Maximum relative error of overall transmission ratio simulation.

In summary, the CVT mechanism characteristics of types I and II were shown in Table 5.

Table 5. CVT mechanism characteristics of types I and II.

Class	Type I: Addition Method			Type II: Multiplication Method	
	A: NG-PBGT	B: NG-PCGT	C: CFG-BG-PCGT	D: CFG	E: NG
Characteristics	Simple design;			Complex design;	
	Larger transmission ratio range;			Smaller transmission ratio range;	
	Less parameter restrictions;			More parameter restrictions;	
	Complex structure;			Simple structure;	
	Large volume			Small volume;	
	Longer transmission chain			Shorter transmission chain	

The type I mechanism has the advantages of simple design, larger transmission ratio range, and less parameter restrictions, while the type II mechanism has the advantages of simple structure, small volume, and shorter transmission chain.

5.2. Transmission Experiment of the Curve Face Gear Pair

In order to verify the correctness of the tooth profile classification design of the curve face gear pair, a transmission experiment is needed. Taking the first pair of the curve face gear pairs in class C as an example, the parameters in Tables 4 and 6 were selected to obtain the curve face gear pairs with three different tooth profiles by 5-axis CNC milling.

Table 6. Specific properties of the curve face gear pair.

Cutting Method	Material	Generating Rack				Curve Face Gear Pair		
		Module	Addendum Coefficient	Coefficient of Bottom Clearance	Pressure Angle	Number of Teeth z_1/z_2	Gears Accuracy Class (ISO)	Circumferential Clearance
5-axis CNC milling	20CrMnTi	4 mm	1	0.25	20°	36/18	8	0.1 mm

Figure 17 shows the transmission experiment of the curve face gear pair. The input rotation speed is 200 rpm, and the load is 50 N·m. The rotation speeds of the input shaft and output shaft were measured by torque-speed sensor JN338 (produced by Beijing Sanjing Creation Science and Technology Group Co., Ltd., Beijing, China) and torque-speed sensor DRFL-VI-500-A-K (produced by ETH-MESSTECHNIK), respectively, and the transmission ratios of three kinds of curve face gear pairs were calculated.

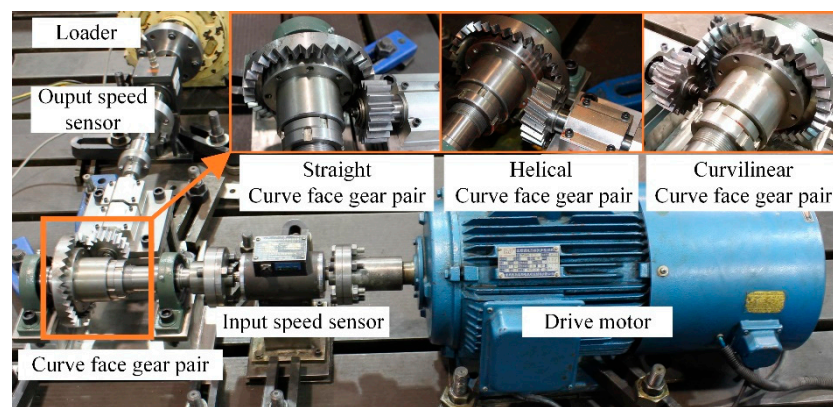


Figure 17. Transmission experiment of the curve face gear pairs with different tooth profiles.

The experimental transmission ratios were compared with the theoretical transmission ratios, as shown in Figure 18. i_t is the theoretical curve of transmission ratio. i_s , i_h and i_c are the measured curves of transmission ratios of curve face gear pairs with straight tooth, helical tooth, and curvilinear tooth, respectively. As can be seen, when the rotational angle θ_2 varies from 0 to 360°, the transmission ratio i_{21} varies in the range of 1.6~2.4, and the number of cycles of i_{21} is 2. Moreover, as can be seen from the total comparison and single comparison, the three measurement curves of the transmission ratio are in good agreement with the theoretical curve, which indicated the correctness of the theoretical method.

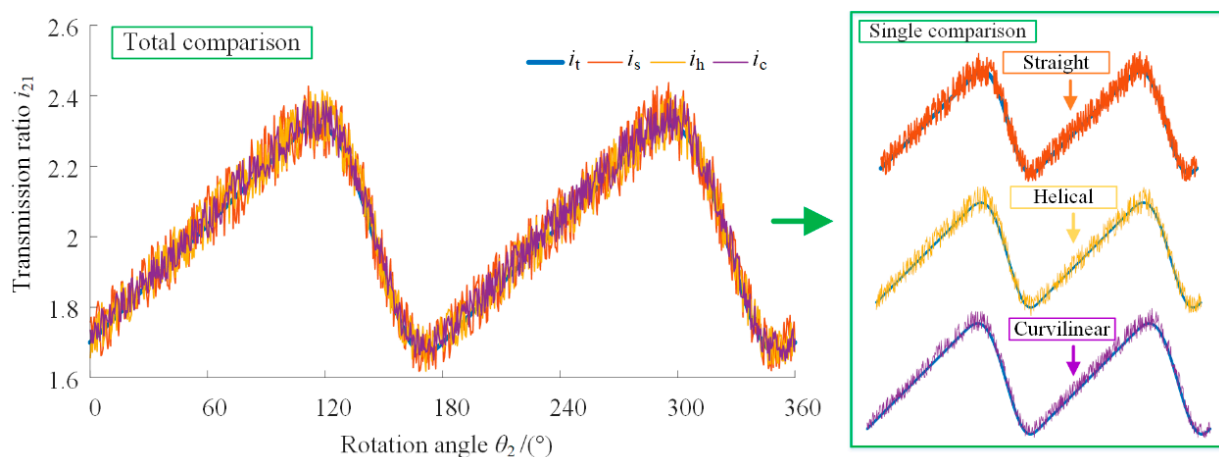


Figure 18. Comparison between the theoretical and experimental transmission ratios of the curve face gear pair.

Figure 19 shows the maximum relative error of the transmission ratio experiment.

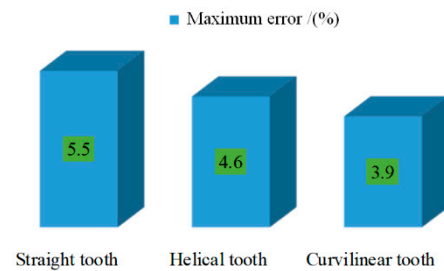


Figure 19. Maximum relative error of the transmission ratio experiment.

The experimental curves of the transmission ratios of the three curve face gear pairs are close to the theoretical curve, and the matching degree from low to high is the transmission ratio curve of the straight tooth, helical tooth, and curvilinear tooth curve face gear pair, respectively. The maximum relative errors of the corresponding transmission ratios are 5.5%, 4.6%, and 3.9%, respectively. The main reason for this difference is that the tooth profile has an important influence on the transmission stability of the curve face gear pair. The curvilinear tooth transmission is the most stable, followed by the helical tooth, and finally the straight tooth.

Besides, the causes of experimental errors mainly include machining errors, installation errors, and measurement errors. Considering the influence of the above errors, the experimental errors were within a reasonable range. The correctness of tooth profile classification design method was verified by the transmission experiment of curve face gear pair, which laid a foundation for the further research of CVT mechanism.

6. Conclusions

Through the study of pattern classification and gear design of spatial noncircular gear CVT, the following conclusions can be drawn.

(1) Under the condition of choosing appropriate parameters, all the five patterns can realize the CVT. Compared with type I, type II has the advantages of a simpler structure, smaller volume, shorter transmission chain, and higher transmission efficiency. However, it is more complex in design, relatively limited by parameters and has a smaller range of transmission ratio. According to the actual working situation and requirements, different patterns can be selected to realize the required CVT;

(2) The curve gear face pair can realize variable transmission ratios between intersecting shafts. Through the tooth profile classification design method, the curve face gear pairs with straight tooth, helical tooth, and curvilinear tooth can be obtained. Compared with the straight tooth curve face gear pair, the helical tooth and curvilinear tooth curve face gear pair have a more complex design, but a greater contact ratio and load capacity, which can meet the requirements of different working situations;

(3) The overall transmission ratio of each pattern was simulated, and the simulation errors were within a reasonable range, which verified the correctness of the theoretical analysis of each pattern. Through transmission experiments, the correctness of the tooth profile classification design method of the curve face gear pair was verified, which provided a strong proof for the correctness of the whole design method to a certain extent;

(4) The CVT principle and transmission ratio characteristics of each pattern were analyzed only from the aspect of kinematics here. However, the dynamic characteristics and performance of each pattern should be further studied in the follow-up work, such as vibration, noise, carrying capacity, and transmission efficiency, which have an important impact on the working performance of the spatial noncircular gear CVT system.

Author Contributions: Conceptualization, Y.Y. and C.L.; data curation, P.X.; formal analysis, Y.Y.; funding acquisition, C.L.; investigation, Y.Y.; methodology, Y.Y.; project administration, C.L.; resources, C.L.; software, Y.Y.; supervision, C.L.; validation, Y.Y.; visualization, Y.Y. and P.X.; writing—original draft, Y.Y.; writing—review and editing, Y.Y. and C.L. All authors have read and agreed to the published version of the manuscript.

Funding: This research was funded by National Natural Science Foundation of China, grant number 51675060.

Institutional Review Board Statement: Not applicable.

Informed Consent Statement: Not applicable.

Data Availability Statement: Not applicable.

Conflicts of Interest: The authors declare no conflict of interest.

Nomenclature

θ_1 and θ_3	Rotation angle of gears 1 and 3 respectively	θ_p ,	Phase angle
i_{21} and i_{43} ,	Transmission ratios of the corresponding gear pairs respectively	i_{oi} ,	Overall transmission ratio between the output shaft and input shaft
i_{7i} ,	Transmission ratio between the bevel gear 7 and the input shaft.	i_{o7} ,	Constant transmission ratio between the output shaft and the bevel gear 7.
i_{Hi} ,	Transmission ratio between the planet carrier H and input shaft.	i_{oH} ,	Constant transmission ratio between the output shaft and the planet carrier H .
i_{o4} ,	Transmission ratio between the output shaft and gear 4.	z_i ,	Teeth number of the corresponding gears
a_1 and b_1 ,	Parameters of the transmission ratios i_{21} of type I.	a_2 and b_2 ,	Parameters of the transmission ratios i_{43} of type I.
K ,	Characteristic parameter of the differential mechanism of type I	a ,	Parameter of the transmission ratios i_{21} and i_{43} of type II.
Φ ,	Maximum rotation angle of noncircular gear 1 in the working area	U ,	The period of the transmission ratio i_{21}
n_1 and n_2 ,	order of noncircular gears 1 and 2 respectively.	n_i and n_l ,	Number of the input gear cycles and branches.
$i'_{01}(\theta_1)$ and $i'_{02}(\theta_1)$,	The first derivatives of $i_{01}(\theta_1)$ and $i_{02}(\theta_1)$ with respect to θ_1 respectively.	$i''_{01}(\theta_1)$ and $i''_{02}(\theta_1)$,	The second derivatives of $i_{01}(\theta_1)$ and $i_{02}(\theta_1)$ with respect to θ_1 respectively.
θ_e ,	Length of the effective working area.	θ_{emin} ,	Minimum length of the effective working area.
$r_1(\theta_1)$ and $r_2(\theta_2)$,	Pitch curve parameter equation of the noncircular gear and curve face gear respectively.	R ,	Projection radius of the pitch curve of curve face gear
V_1 and V_2 ,	Speeds at the meshing points of the two curves respectively	ω_1 and ω_2 ,	Angular speeds of the two gears, respectively
β_r and b_r ,	The helical angle and tooth width parameter of the helical rack respectively	θ_r and ρ_r ,	The arc angle and arc radius of the curvilinear rack respectively.
$r_r(u_r, b_r, \theta_r)$,	Tooth surface equations of the generating rack with three kinds of tooth profiles in S_r	$r_c(u_r, b_r, \theta_r)$,	Tooth surface equations of the generating gear with three kinds of tooth profiles in S_c
σ_c, σ_1 and σ_2 ,	Pitch curve of the generating gear, noncircular gear, and curve face gear respectively	θ_c ,	Rotation angle of the generating gear around its own axis.
$r_1(u_r, b_r, \theta_r, \theta_1)$,	Tooth surface equation of noncircular gear with three kinds of tooth profiles in S_1	$r_2(u_r, b_r, \theta_r, \theta_1)$,	Tooth surface equation of curve face gear with three kinds of tooth profiles in S_2

References

1. Litvin, F.L.; Fuentes, A. *Gear Geometry and Applied Theory*; Cambridge University Press (CUP): Cambridge, UK, 2004; pp. 318–348.
2. Addomine, M.; Figliolini, G.; Pennestri, E. A landmark in the history of non-circular gears design: The mechanical masterpiece of Dondi's astrarium. *Mech. Mach. Theory* **2018**, *122*, 219–232. [[CrossRef](#)]
3. Liu, J.-Y.; Chang, S.-L.; Mundo, D. Study on the use of a non-circular gear train for the generation of Figure-8 patterns. *Proc. Inst. Mech. Eng. Part C J. Mech. Eng. Sci.* **2006**, *220*, 1229–1236. [[CrossRef](#)]
4. Mundo, D. Geometric design of a planetary gear train with non-circular gears. *Mech. Mach. Theory* **2006**, *41*, 456–472. [[CrossRef](#)]

5. Mundo, D.; Gatti, G.; Dooner, D. Optimized five-bar linkages with non-circular gears for exact path generation. *Mech. Mach. Theory* **2009**, *44*, 751–760. [[CrossRef](#)]
6. Ottaviano, E.; Mundo, D.; Danieli, G.; Ceccarelli, M. Numerical and experimental analysis of non-circular gears and cam-follower systems as function generators. *Mech. Mach. Theory* **2008**, *43*, 996–1008. [[CrossRef](#)]
7. Modler, K.-H.; Lovasz, E.-C.; Bär, G.; Neumann, R.; Perju, D.; Perner, M.; Mărgineanu, D. General method for the synthesis of geared linkages with non-circular gears. *Mech. Mach. Theory* **2009**, *44*, 726–738. [[CrossRef](#)]
8. Alexandru, P.; Macaveiu, D.; Alexandru, C. A gear with translational wheel for a variable transmission ratio and applications to steering box. *Mech. Mach. Theory* **2012**, *52*, 267–276. [[CrossRef](#)]
9. Zheng, F.; Hua, L.; Han, X.; Li, B.; Chen, D. Synthesis of indexing mechanisms with non-circular gears. *Mech. Mach. Theory* **2016**, *105*, 108–128. [[CrossRef](#)]
10. Yu, Y.; Lin, C.; Hu, Y. Study on simulation and experiment of non-circular gear surface topography in ball end milling. *Int. J. Adv. Manuf. Technol.* **2021**, *114*, 1913–1923. [[CrossRef](#)]
11. Lin, C.; Gong, H.; Nie, N.; Zen, Q.; Zhang, L. Geometry design, three-dimensional modeling and kinematic analysis of orthogonal fluctuating gear ratio face gear drive. *Proc. Inst. Mech. Eng. Part C J. Mech. Eng. Sci.* **2012**, *227*, 779–793. [[CrossRef](#)]
12. Lin, C.; Zeng, D. Design, generation and tooth width analysis of helical curve-face gear. *J. Adv. Mech. Des. Syst. Manuf.* **2015**, *9*, JAMDSM0066. [[CrossRef](#)]
13. Lin, C.; Yu, Y.; Hu, Y. Analysis of composite motion law and force of high speed curve-face gear. *J. Adv. Mech. Des. Syst. Manuf.* **2017**, *11*, JAMDSM0070. [[CrossRef](#)]
14. Yu, Y.; Lin, C.; Hu, Y. Tooth bending stress analysis of high speed curve face gear of composite transmission. *Mech. Ind.* **2021**, *22*, 20. [[CrossRef](#)]
15. Hu, Y.; Lin, C.; Li, S.; Yu, Y.; He, C.; Cai, Z. The Mathematical Model of Curve-Face Gear and Time-Varying Meshing Characteristics of Compound Transmission. *Appl. Sci.* **2021**, *11*, 8706. [[CrossRef](#)]
16. Dooner, D.; Yoon, H.-D.; Seireg, A. Kinematic considerations for reducing the circulating power effects in gear-type continuously variable transmissions. *Proc. Inst. Mech. Eng. Part D J. Automob. Eng.* **1998**, *212*, 463–478. [[CrossRef](#)]
17. Sun, C.Q.; Sun, G.X.; Ren, A.H.; De Liu, Y. The Kinematic Analysis of Heart-Shaped Gear Continuously Variable Transmission. *Appl. Mech. Mater.* **2010**, *37*, 1489–1492. [[CrossRef](#)]
18. Wang, X.F.; Zhu, W.D. Design, Modeling, and Simulation of a Geared Infinitely Variable Transmission. *J. Mech. Des.* **2014**, *136*, 071011. [[CrossRef](#)]
19. Zhu, W.D.; Wang, X.F. Modeling and Control of an Infinitely Variable Speed Converter. *J. Dyn. Syst. Meas. Control* **2014**, *136*, 031015. [[CrossRef](#)]
20. Wang, X.F.; Zhu, W.D. Design, Modeling, and Experimental Validation of a Novel Infinitely Variable Transmission Based on Scotch Yoke Systems. *J. Mech. Des.* **2016**, *138*, 015001. [[CrossRef](#)]
21. Chen, S.; Dong, Z. Transmission characteristics and phase number optimization on the transmission mechanism of rod gear pulse continuously variable transmission. *Adv. Mech. Eng.* **2018**, *10*, 1687814017751966. [[CrossRef](#)]